Research Square

Preprints are preliminary reports that have not undergone peer review.
They should not be considered conclusive, used to inform clinical practice,
or referenced by the media as validated information.

Detection of burned areas with extreme gradient boosting algorithm in a multi-temporal setting (MBAGB)

Ana Militino (militino@unavarra.es)
Public University of Navarre: Universidad Publica de Navarra https://orcid.org/0000-0002-0631-3919
Harkaitz Goyena
Public University of Navarre: Universidad Publica de Navarra
Unai Pérez-Goya
Public University of Navarre: Universidad Publica de Navarra
Maria Dolores Ugarte
Public University of Navarre: Universidad Publica de Navarra

Research Article

Keywords: commission error, deep learning, machine learning, MODIS, omission error, spectral indexes, VIIRS, XGboost

Posted Date: March 17th, 2022

DOI: https://doi.org/10.21203/rs.3.rs-1445331/v1

License: This work is licensed under a Creative Commons Attribution 4.0 International License.
Read Full License

Detection of burned areas with extreme gradient boosting algorithm in a multi-temporal setting (MBAGB)

A. F. Militino[1*†], H. Goyena[1†], U. Pérez-Goya[1†] and M. D. Ugarte[1†]

[1]Department of Statistics, Computer Science and Mathematics and Institute for Advanced Materials and Mathematics (InaMat^2) (Spain), Public University of Navarra, Campus de Arrosadia, Pamplona, 31006, Navarre, Spain.

*Corresponding author(s). E-mail(s): militino@unavarra.es;
Contributing authors: harkaitz.goyena@unavarra.es;
unai.perez@unavarra.es; lola@unavarra.es;
†These authors contributed equally to this work.

Abstract

Wildland fires are one of the most important disturbances on Earth ecosystems, where the combination of remote sensing data and modern machine learning techniques offer a great potential for detection and monitoring of burned areas. Many algorithms have been developed in parallel to locate burned areas at local and global scales, but more accurate methodologies are still needed to provide precise and valuable information to climate users, environmentalists and public administrations. Gradient boosting-based methodologies have shown a good performance when dealing with segmentation of burned areas. In this paper, we propose a new method, called MBAGB, based on these methodologies for detecting and mapping burned areas in a multi-temporal setting of satellite imagery. We illustrate the procedure with the fires occurred in October 2017 in a region covering the North-Central Portugal and the North-West of Spain. Daily satellite images used for the definition of spectral indexes are taken from MODIS satellite products, between September and November 2017. The MBAGB accuracy metrics show the overall goodness of this method, and in particular, a very small number of false negatives in the identification of burned areas.

Keywords: commission error; deep learning; machine learning; MODIS; omission error; spectral indexes; VIIRS; XGboost

1 Introduction

Identification and mapping of burned areas are essential tasks for monitoring the Earth surface, where satellite images are crucial sources of information [1, 2]. More specifically, the generation of global burned area (BA) products has been an important issue since the late 1990s, but only since the 2000s we can find periodical and global BA products routinely derived with different degrees of accuracy, yet not for all over the Earth.

The Moderate Resolution Imaging Spectroradiometer (MODIS) provides free access to the MCD64A1 version 6 of burned area (BA) data as a monthly global gridded 500m product containing per-pixel burned-area and quality information [3]. The surface reflectance imagery is jointly combined with 1km MODIS active fire observations. The algorithm used for creating this product lies in a burn sensitive vegetation index (VI) to create dynamic thresholds, yet some disturbances caused by clouds, atmospheric absorption and sensor-introduced noises can still be present [4]. There are specific contributions for detecting BA products with Landsat and Sentinel missions, but regrettably they are only available in some regions of the Earth. In the conterminous United States (1984 - 2015) there are Landsat BA products such as Landsat Burned Area Essential Climate Variable (BAECV) publicly available [5], and Landsat Burned Area [6]. In Sub Saharan Africa specific algorithms have been also developed using both the information of MODIS active fires and Sentinel-2 MSI reflectance measurements [7, 8]. On tropical Africa, optical-based algorithms provide a significant performance over the radar-based algorithms [9]. Sentinel 3 offers products for mapping burn scars through the identification of surfaces sufficiently affected by fire [10].

Satellite products are based on a great variety of algorithms with different efficiencies depending on image resolutions and ecosystem variety, yet recently the fast evolution of deep learning and machine learning methods have enabled to improve the detection of burned areas [11] or the study of wildfire spread patterns [12]. Commonly, a burned vegetation index is created for allowing the identification of burned and unburned areas defined on different thresholds after filtering low-quality pixels, and then combining this information with active fires. The use of different auxiliary information as input attribute is also frequent [13]. Very well known methods as random forest [14, 15], support vector machines [16, 17], artificial neural networks [18], convolutional neural networks with long short term memory (LSTM) [19], BA-Net deep learning method [20], U-net convolutional neural networks [21], geometric semantic genetic programming [22] and XGBoost [23, 24] are now popular methods for segmentation of burned regions.

In this paper, we explore the capabilities of the extreme gradient boosting algorithm (XGBoost) [25] as a machine learning method that can be specifically designed for classification of very imbalanced data. The whole procedure, called MBAGB, optimises the detection of burned areas in a multi-temporal mapping, where the difference between pre-burned and post-burned area spectral indexes are used to identify the magnitude and location of burn scars [26].

Figure 1 shows the flowchart of the method divided in four steps. The first one consists of the database collection made with thermal anomalies, the european forest fire information system (EFFIS) of burned areas perimeters, the surface reflectance of the satellite images, and the land cover classification. This step is explained in Section 2. Steps 2 and 3 are reported in Section 3, with the generation of auxiliary attributes based on difference of spectral indexes in Subsection 3.1, and the process of tuning the hyperparameters of the XGBoosting algorithm in Subection 3.2. Step 4 shows the results based on the validation process, that are detailed in Section 4. The paper finishes with the discussion in Section 5 and the conclusion in Section 6.

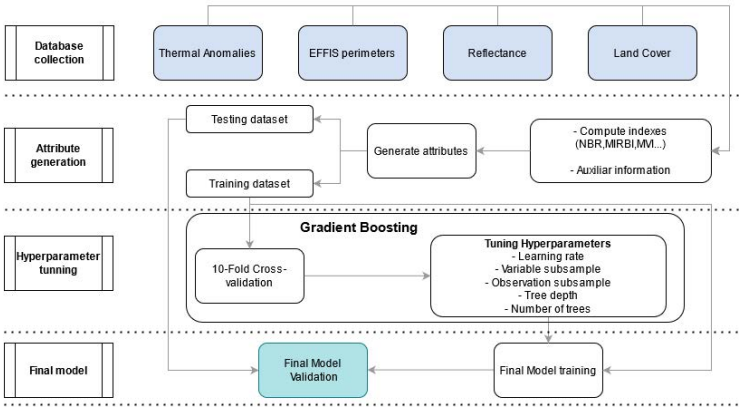


Fig. 1 Flowchart for detecting burned areas with extreme gradient boosting algorithm (MBAGB).

2 Data and Study Region

Galicia is a region of roughly 30,000 km^2 located in the north of Spain and above Portugal, that concentrates the highest number of fires in Spain. Almost 30% of Spanish fires are in Galicia region with a yearly average of 11,000 fires. In 2017, the 80% of the 620 km^2 burned in Galicia were dated in 2 days, where more than 20 fires burned surfaces were greater than 5 km^2. Portugal has about 92,090 km^2. More than two thirds of this surface is covered by forests, but 97% belongs to private companies. In Portugal, there are between 15,000 and 25,000 wildland fires each year burning from 1,500 to 2,500 km^2 [27]. The

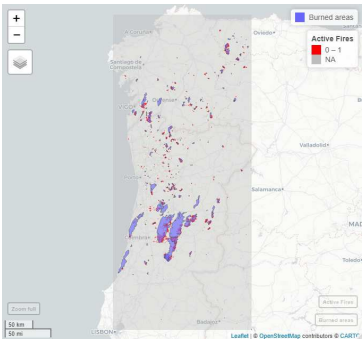


Fig. 2 Burned areas from EFFIS data base in blue, thermal anomalies of MCD14DL and active fires from VIIRS in red. The shadowed region is the region of interest.

region of interest covers Galicia plus the north and central region of Portugal, with an extension of about 108,321 km^2. MODIS, splits the Earth in 460 non-overlapping tiles of approximately $10° \times 10°$ using the sinusoidal projection (SR-ORG:6974). Getting the entire region requires downloading two MODIS tiles every date (see shadowed region of Figure 2).

Additionally, more products are necessary for the definition of the classification reference and input attributes in the burned detection process:

- The surface reflectance products MOD09GA and MYD09GA version 6 coming from Terra and Aqua satellites. These products are the foundation for the spectral indexes described in Section 3.1, and they are the source images of many land MODIS products. Terra crosses the Equator every day at 10h30 a.m. and Aqua at 1h30 p.m. at the same orbit, therefore, the three hours lag between both satellites can complement the missing pixels of one satellite image with the other satellite image pixels in the same day. This multispectral images contains 7 bands of the surface spectral reflectance at 500m of spatial resolution. We draw them in the two tiles of both satellites from the 91 days of September, October and November 2017.
- The land cover product MCD12Q1 of 2016, because 2016 is the last available land cover product before the 2017 fires. This product provides yearly land cover maps at 500m of spatial resolution with 17 classification legends. From these data we create a filter to categorize the pixels as burnable (0) and unburnable (1). We assign as burnable the following legends: croplands (legend 12), urban and built-up lands (legend 13), croplands and natural vegetation (legend 14), permanent snow and ice (legend 15), barren (legend 16), water bodies (legend 17) and unclassified (legend 18). The rest are categorized as burnable. Therefore, we create a mask that identifies the burnable potential pixels from the un-burnable ones.
- The fires location product MCD14DL of October 2017. This is a monthly product of near real-time (NRT) MODIS Thermal Anomalies or fire locations representing the center of a 1km pixel of spatial resolution that allows to identify fires and other termal anomalies such as volcanoes. The pixels

are flagged by the MODIS MOD14/MYD14 Fire and Thermal Anomalies algorithm [28].

- The visible infrared imaging radiometer suite (VIIRS) of October 2017. It is a sensor launched on the Suomi-National Polar-orbiting Partnership satellite (S-NPP) on October 28, 2011, to replace the AVHRRs on the NOAA satellites. It detects active fires and other thermal anomalies [29] providing a means to identify fire-induced changes in surface reflectance [30]. VIIRS data complements MODIS (MCD14DL) fire detection. Both sources provide vector files [31].
- The burned area product EFFIS wildfire data base of October 2017 [32]. It contains perimeters of burned areas in Europe since 2003 in vector files. This product is derived from the daily processing of MODIS satellite imagery at 250m ground spatial resolution. The perimeters of the burned scars are detected from MODIS satellite imagery. They can plot burnt scars of approximately 30 hectares in size but smaller sizes are also included. The perimeter burnt areas in blue, and the thermal anomalies or active fires in red are plotted in Figure 2.
- The burned area final product MCD64A1 version 6 of October 2017. It is a combination of Terra and Aqua burned areas of monthly images of 500m. It uses the atmospherically-corrected level reflectance products 2G daily surface [33]. Every scene contains per-pixel burned area and quality information. Layers include burned day, burned data uncertainty and quality indicators. This product is used for comparison purposes of the proposed method MBAGB.

After downloading these products we intersect them with the region of interest.

3 Methods

The MBAGB method needs merging the information coming from the EFFIS burned areas data base, and the spectral indexes for defining the reference classification variable and the input attributes. The classification reference is a binary variable that takes the value 0 when the location is not burned and 1 when it is burned. It is considered as ground truth data. This variable and the input attributes are defined with the spectral indexes derived from MODIS satellite imagery, that evaluate the surface reflectance change [34], the land cover mask of burnable pixels, and the distances from each pixel to the nearest fires (distAF). We first define the spectral indexes.

3.1 Spectral Indexes

The spectral indexes are given by the combination of spectral bands aimed at measuring changes due to burning. The spectral reflectance of both MOD09GA and MYD09GA products provide the required bands for this study: band 1 (red), band 2 (near infrared), band 5 (shortwave-infrared 1), band 6

(shortwave-infrared 2) and band 31 (thermal infrared TIRS1), denoted by R, NIR, SWIR1, SWIR2 and TIRS1, respectively. Table 1 shows the definition of the spectral indexes, and the pre-fire and post-fire differences used in this study.

Table 1 Definitions of the spectral indexes and pre-fire and post-fire differences identified with the suffixes pre and post respectively

Spectral indexes	Definition	Difference index
NBR	$\frac{NIR - SWIR2}{NIR + SWIR2}$	$dNBR1 = NBR_pre - NBR_post$
NBR2	$\frac{SWIR1 - SWIR2}{SWIR1 + SWIR2}$	$dNBR2 = NBR2_pre - NBR2_post$
MVI	$\frac{TIRS1 - SWIR2}{TIRS1 + SWIR2}$	$dMVI = MVI_pre - MVI_post$
MIRBI	$10 \times SWIR2 - 9.8 \times SWIR1 + 2$	$dMIRBI = MIRBI_pre - MIRBI_post$
NIR	Near Infrared band	$dNIR = NIR_pre - NIR_post$

The normalized burn ratio (NBR) is the most popular, originally developed for identifying burned areas [35], and later used for burn severity assessment [36]. It is defined with two spectral bands, the near-infrared and the shortwave-infrared wavelength, both sensitive to burning but in opposite way. It generally ranges between -1 and 1. The rest of the indexes are also very sensitive to the changes in live green vegetation or moisture content: The normalized burn ratio 2 (NBR2) [37, 38], the burn-sensitive vegetation index (MVI) [39], the mid infrared bispectral index (MIRBI) [40, 41]. We also use the near infrared (NIR) band 2 of MODIS, commonly used for monitoring temporal burn signatures [42, 43]. Higher values of these indexes are associated with high severity, and negative values are associated with regrowth after the fire. Values close to zero are associated with non-burned areas. All of these indexes decrease significantly after a fire, becoming good indicators of burned pixels [44].

In multi-temporal analysis, where time series of images are available, difference of spectral indexes are a frequent tool in change detection algorithms for identifying burned areas [45, 46]. The difference process consists in subtracting the index value of the posterior (post) date from the previous (pre) value of the detected fire [47].

3.2 The eXtreme Gradient Boosting method (XGBoost)

The eXtreme Gradient Boosting procedure (XGBoost) is an advanced implementation of the gradient boosting method [48, 49]. It is an ensemble learning method and supervised algorithm, because a single model combines the predictive power of multiple learners. The main ensemble learners are boosting and bagging, both usually based on decision trees, that predict the target variable through several input attributes.

Boosting works with sequential trees reducing errors from previous trees, and it is appropriate for managing large sets of data without specified assumptions. The main advantages of the decision trees are the relative simple structure, the lack of assumptions, and the flexibility and robustness with regard to other methods [50]. Decision trees can handle nonlinear relationships between features and classes, they work with missing values and they can manage categorical and numerical values. Moreover, they do not assume independence among predictors, and thus they can handle with dependent variables.

The gradient boosting method is used for producing stronger learners. The main difference with other bagging methods as random forest, is that boosting uses trees with few splits. In the training step the parameters of the weak learner are fitted iteratively minimising an objective function such as the proportion of errors or the root mean squared error among others. Every learner is compared with its previous learners with stopping criterion that avoids overfitting. XGBoost has been implemented through the `xgboost R` package [51], yet we have also used `rsat` [52] and dependent packages for downloading, customising and managing the images, vector and text files. For the definition of the classification reference attribute and the input attributes necessary for running the MBAGB model we proceed as follows.

3.2.1 Preparing indexes

The `rsat` package helps to define the indexes. It also ensambles the images by its region and time of interest in a object called *rtoi*, that includes Galicia and the Portuguese regions of Santarém, Braga, Vila Real, Coimbra, Guarda, Aveiro, Viseu, Castelo Branco, Portalegre, Braganca, Porto and Viana do Castelo. See Figure 2 for the location in the Iberian peninsula. We create a multilayer called stack with the 91 multispectral images from MOD09GA and the 91 images from MYD09GA (Terra and Aqua respectively) of September, October and November 2017, necessary for defining the indexes NBR, NBR2, MIRBI, MVI and NIR band (hereafter managed as another index). Then, the Terra and Aqua daily cloud masks are intersected with every layer of the raster for identifying the clouds. These pixels are defined as missing pixels, and then excluded in the classification process. The composite images of indexes are made by covering the indexes defined with MOD09GA with the corresponding indexes defined with MYD09GA. It means that we substitute unavailable pixels of MOD09GA indexes with available MYD09GA pixels for the corresponding indexes, reducing the number of unavailable or erroneous pixels. Gapfilling methods are also recommended for smoothing the images [53–55]. After downloading the landcover scene of 2016 from MCD12Q1, we extract the data from the *rtoi*, and create a binary mask for reclassifying the first 11th categories (from a total of 17) in the new category of burnable pixels, and the rest in the category of unburnable pixels. The new classification is used for filtering the composite image of indexes.

3.2.2 Active Fires

Using the vector file of active fires of October 2017 from MDC14DL and VIIRS sensors in the *rtoi*, we obtain the nearest active fires date using the Dirichlet tesselation, and we define a raster with the distance (distAF) of every pixel in the raster to the nearest active fire. The Dirichlet tesselation creates a polygon around a center point where any other point inside the polygon is closer to the center point than any other point. Then, all the pixels in the same polygon have assigned the same date of the closer fire. The dates of fire are used for identifying the 8 previous and the 8 posterior available images for every pixel. These images are drawn from the time series of indexes already defined between September and November 2017. Next, we calculate the difference indexes subtracting the median of the 8 previous dates minus the median of the 8 posterior date of fires. The amplitude of 8 days is empirically the most convenient for our time series of images, but it can be changed according to the number of available images, because dates do not need to be sequential. The fire date can be different for every pixel. We prepare a multilayer raster with layers of the difference indexes (dNBR1, dNBR2, dMIRBI, dMVI, and dNIR), the mask of the burnable and unburnable pixels, the distances of every pixel to the next active fire and the landcover classification.

3.2.3 Classification Reference

The classification reference attribute is a binary variable with burned pixels (1) and unburned pixels (0). The burned pixels are drawn from the EFFIS data base of burned areas greater than 2 km^2 and $dNBR > 0.1$. The unburned pixels are the rest of the pixels with $dNBR1 \leq 0.15$ for avoiding isolated fires not identified in the EFFIS database [36]. These thresholds can be tuned according to the spatial resolution images.

Next, we prepare the input text file with the input attributes: difference spectral indexes (dNBR1, dNBR2, dMVI, dMIRBI, and dNIR), distance to the nearest active fire (distAF), landcover of burnable pixels, and the reference classification attribute. The input file has around .5 million of features. In the training process we randomly choose 75% of these features and run the XGBoost algorithm for a family of hyperparameters, where one of those is specifically designed for handling imbalanced data. The stopping criterion consists in minimizing the root mean squared error, a common measure for evaluating the predictive ability of learning algorithms. Finally, we obtain a confusion matrix of the classification results, from which we calculate the accuracy metrics of Table 2. In the confusion matrices, the number of analyzed pixels are distributed according to the matches of the reference classification data and the MBAGB classification method. The true positives (TP) indicate the matches of pixels that are both defined and predicted as burned pixels. The false negatives (FN) are those pixels that are defined as burned pixels but predicted as unburned. The false positives (FP) are those defined as unburned pixels but predicted as burned, and finally the true negatives (TN) are those

defined and predicted as unburned pixels. Therefore, the detection rate is the proportion of correctly classified pixels, the omission error is the rate of undetected pixels over the reference set, and the commission error is the proportion of uncorrected detected pixels over the reference classified set. The precision is the rate of detected and true burned pixels over the MBAGB burned classified pixels. It is also the complement of the commission error ($P = 1 - CE$). The recall or sensitivity is the proportion of the detected and true burned pixels over the reference classified pixels. It is the complement of the omission error ($R = 1 - OE$). The Dice coefficient is a similarity measure lying between 0 and 1. When it is close to 1 two criteria are met. The reference and the predicted classification are similar in size, and there is a high degree of overlap between both [56]. The kappa coefficient (κ) is a measure of the agreement between the two raters, the reference and the classifier.

Table 2 Definition of accuracy metrics

Detection Rate (D)	$D = \frac{TP}{TP + TN + FP + FN}$
Omission Error (OE)	$OE = \frac{FN}{TP + FN}$
Commission Error (CE)	$CE = \frac{FP}{TP + FP}$
Precision (P)	$P = \frac{TP}{TP + FP}$
Recall (R)	$R = \frac{TP}{TP + FN}$
Dice coefficient (DC)	$DC = \frac{2TP}{2TP + FN + FP}$
kappa (κ)	$\kappa = \frac{P_0 - P_e}{1 - P_e}$ *
Overall Accuracy (OA)	$OA = \frac{TP + TN}{TP + TN + FP + FN}$

* P_0 is the relative observed agreement between reference and XGboost assessments and P_e is the hypothetical probability of chance agreement.

4 Results

The validation process of the MBAGB procedure is based on the interpretation of confusion matrices and the accuracy metrics. Table 3 provides the predicted classified pixels versus the reference classified pixels. The confusion matrices are first calculated in the test set defined with the 25% of remaining features of the full dataset, second in the whole full data set, and third in the MCD64A1 image of MODIS burned area product. XGBoost procedure learns to reduce the number of false negatives (FN) and gives the same number of 81 FN in the test set and in the full dataset. When the predicted classification is made on

the MCD64A1, the number of FN increases to 800. This is an expected behavior, because this is an external classification only used for validation purposes. Table 4 gives the proportions of TP, TN, FP and FN over the total number of pixels analyzed in the test set (126168), the full dataset (504672), and the MCD64A1 (504672) set, simplifying the interpretation of the confusion matrix. The detection rate of burned pixels is 3.1%, 3.1% and 2.7% in the training dataset, full dataset, and MCD64A1 respectively. The percentages of TP and TN are lower in MCD64A1 product than in the test and full dataset, but the percentages of FN (0.002) and FP (0.004) are higher. Then, the MBGAB predicted classification detects a higher proportion of burned pixels than the product provided by MODIS, and lower percentage of FP and FN. Moreover, the determination coefficient R^2 of the MBAGB classification versus the reference classification is 0.979 and the R^2 of the MBAGB classification versus the MCD64A1 classification is 0.81.

Table 3 Estimated confusion matrices with MBAGB versus the reference classification over the test set, the full data set and the MCD64A1 BA product

		MBAGB		
Reference		Burned	Unburned	Total
Test set	Burned	3894 (TP)	81 (FN)	3975
	Unburned	144 (FP)	122049 (TN)	122193
Full set	Burned	15819 (TP)	81 (FN)	15900
	Unburned	239 (FP)	488533 (TN)	488772
MCD64A1	Burned	13874 (TP)	800(FN)	14674
	Unburned	2184 (FP)	487814 (TN)	489998

Table 5 shows the accuracy assessment of the MBAGB predicted classification. The overall accuracy is very high in the three scenarios, and the corresponding omission errors are very low: 0.020, 0.005 and 0.055 respectively. The reduction of omission error induces an increase in the commission error, but the priority of the study is the detection of fires minimizing the underestimation of false negatives. Clearly, in the MCD64A1 dataset the accuracy metrics are not so competitive as in the test and full data sets, but the MBAGB ability is proven to be satisfactory with new datasets.

Table 4 Proportions of True Positives (TP), True Negatives (TN), False Negatives (FN) and False Positives (FP) predicted with MBAGB in the test set, the full dataset and MCD64A1 Burned areas Modis product.

	MBAGB			
	TP	TN	FN	FP
Test set	0.031	0.967	0.001	0.001
Full set	0.031	0.968	0.000	0.000
MCD64A1	0.027	0.967	0.002	0.004

Figure 3 shows the predicted classification in two panels. On the left, the MBAGB prediction vs. the reference classification considered as ground truth

Table 5 Estimated accuracy metrics of MBAGB predicted classification versus the reference classification over the test set, the full set, and the specific MCD64A1 product of burned areas of MODIS.

		MOD09GA/MYD09GA	
Metrics	test	Fulldataset	MCD64A1
Detection Rate	0.031	0.031	0.027
Omission error	0.020	0.005	0.055
Commission error	0.036	0.015	0.136
Precision	0.964	0.985	0.864
Recall	0.980	0.995	0.945
Dice coef	0.972	0.990	0.903
κ	0.971	0.990	0.900
Overall Accuracy	0.998	0.999	0.994

classification, and on the right, the MBAGB prediction vs. the MCD14A1 classification of burned area MODIS product. In both panels the TN or green pixels are the unburned pixels identified with the reference classification, the MBAGB prediction, and the MCD64A1 classification. The burned pixels or TP pixels (in blue) show a great coincidence in both panels for the majority of burn scars. Only some false negatives (FN)(plotted in red) and false positives (FP) (plotted in yellow) are observed as misclassified pixels, many of them in the border regions of burned pixels, and more frequent in the right panel. Overall, the MBAGB predicted classification is very satisfactory over the reference classification, not only in the high number of TP and TN pixels, and the small number of FP and FN, but also in their matching locations. There is also a good performance of MBAGB over the MCD64A1 product, yet more false negatives are observed.

Figure 4 zooms the highlighted region of Figure 3. The blue burned scars are well identified in both panels, except for a small spot inside the largest burn scar, where some pixels are identified as green on the left panel (or true negatives, meaning that they are unburned pixels by MBAGB prediction and reference classification), and identified as red on the right panel (or false negatives, meaning that they are predicted with MBAGB as unburned pixels but MCD64A1 identifies as burned). On the right panel we can also observe more false positives (in yellow) that in the left panel, but most of them are in the border of burn scars.

Figure 5 plots the partial contribution of the input variables to the MBAGB classification method in decreasing order. The dNBR1 variable has the largest contribution in the classification process, followed by dMVI, dNIR, distAF, dNBR2, dMIRBI and landcover. This range of contribution is expected, because dNBR1 is crucial for the definition of reference classification and dMVI is used in the definition of MODIS BA products [3]. The other indexes and attributes are less important but they are also needed for improving the classification.

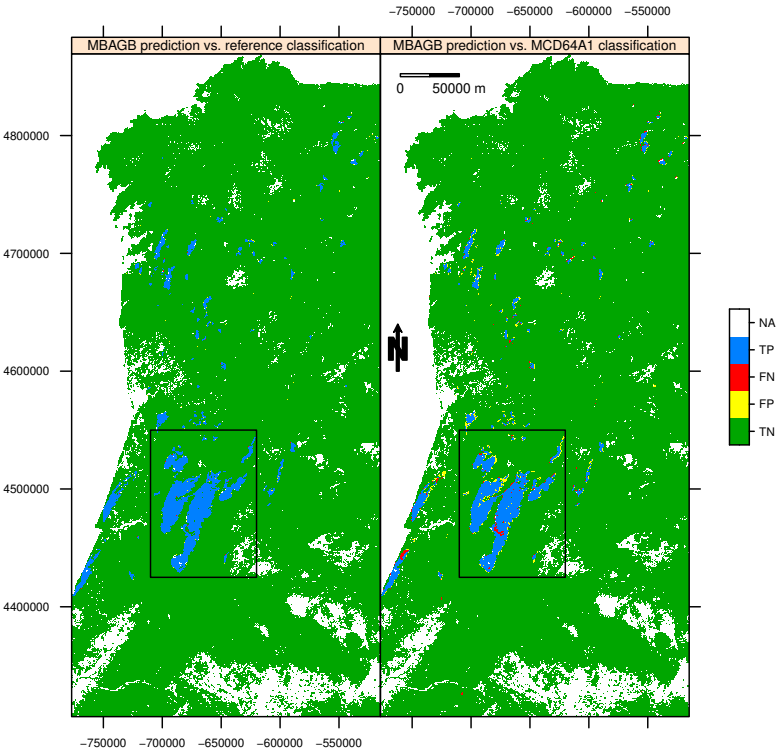


Fig. 3 On the left panel, the MBAGB prediction vs. the reference classification, and on the right panel, the MBAGB prediction vs. the MCD64A1 burned area MODIS product. NA pixels are missing data, and TP, FN, FP and TN are the true positive, false negative, false positive and true negative pixels detected in the classification. The highlighted region is zoomed in Figure 4

5 Discussion

MBAGB is a recommended procedure for calibrating burned areas identification when we are interested in reducing the number of false positives. It is easy and fast to implement, and can be used in any region of the Earth. It can also be adapted to higher temporal and spatial resolution images yet it will be more time-consuming. The procedure has also some limitations, for example, it is true that model performance has an inherent uncertainty, for example if different datasets are used for testing models, then each metric must be seen as a realisation of a random variable with a given distribution, and statistical inferences can be made for checking statistical differences. Covariates used as input attributes could vary depending on the study region, quality of data or

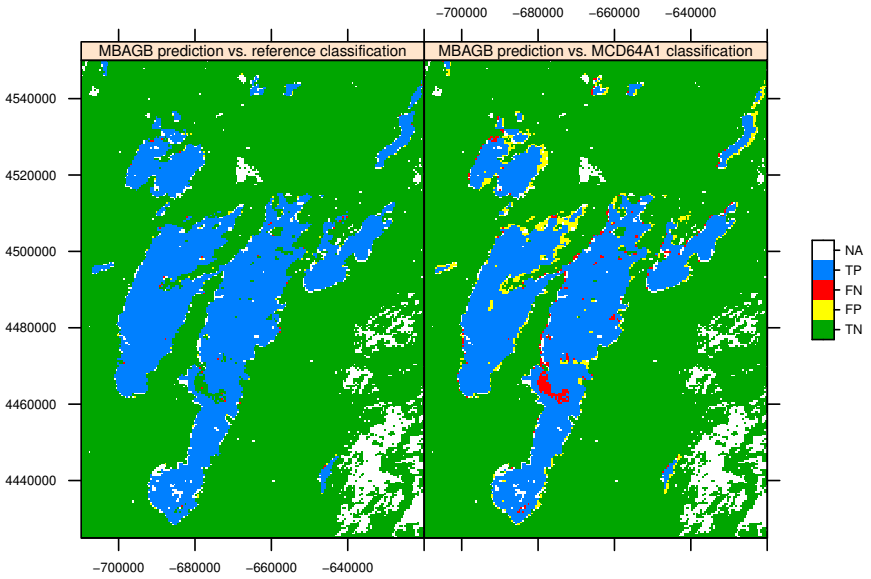


Fig. 4 On the left panel, the MBAGB prediction vs. the reference classification, and on the right panel, the MBAGB prediction vs. the MCD64A1 burned area MODIS product in the highlighted region of Figure 3. NA pixels are missing data, and TP, FN, FP and TN are the true positive, false negative, false positive and true negative pixels detected in the classification.

time period, hence a previous check of the auxiliary information availability is necessary. The classification accuracy may be measured with different metrics of the root mean squared method such as binary classification error rate, negative log-likelihood function, mean absolute error, mean absolute percentage error or area under the ROC curve (AUC). All of them provide similar results, but it is acknowledged that the AUC criterion is not recommended for very imbalanced data sets [57]. XGBoost model exhibits higher accuracy than single decision trees, but the interpretability is also more difficult. Other machine learning methods such as support vector machines, random forest or neural networks can also be used, yet XGBoost shows also a good performance even for detecting burned areas with Landsat imagery [58].

6 Conclusion

Detection and mapping of burned areas are a major concern subject for climatologists, environmentalists, forestry engineers, governments and communities

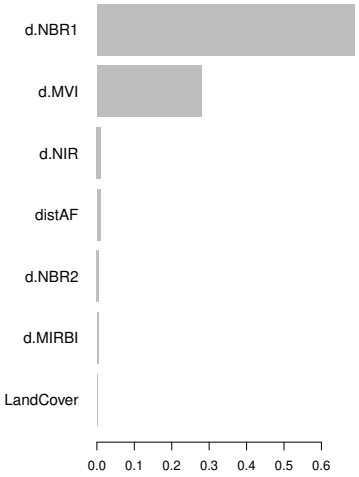


Fig. 5 Importance matrix of the partial contribution of input variables to the MBAGB classification method.

for diverse ecological, social and economic reasons. Nowadays, the free access to time-series of satellite images makes it easier the identification of these areas not only in accessible places, but also in remote areas where there are many unreported fires. Optical sensors provide a rich data mine of information, but they are not free of noise caused by atmospheric or technical reasons. Therefore, the combination of information coming from different sources is a way to reduce the errors and to increase the overall accuracy, even in coarse resolution images. This accuracy can be improved with new algorithms and the use of machine learning techniques. In this work, we contribute to this aim by using the MBAGB method based on the extreme gradient boosting method (XGBoost) applied to MOD09GA/ MYD09GA images. We need a reference classification based on EFFIS BA perimeters, and the constraints of some values of the dNBR1 index. The definition of difference spectral indexes requires the location and dates of active fires from VIIRS and MCD14DL products, and the identification of burnable and unburnable pixels through the MCD12Q1 landcover. The reference classification can be interpreted as ground truth data, so it is expected that the MBAGB procedure classify properly the test set and the full data set. However, we also check the MBAGB high performance over a new data set, the MCD64A1 burned area MODIS product. The absence of these products in Landsat or Sentinel platforms, hinders the definition of a new reference classification based on higher spatial and lower temporal resolution images, but MBAGB method could be also be fitted to these images with the reference classification based on MODIS. The MBAGB method shows not only a good performance through the confusion matrices and accuracy measures, but also a high runtime performance for improving the detection of burned areas in the north region of Spain and Portugal. Both areas unfortunately affected by many fires in October 2017. The method reaches a desirable

high number of true positives (TP) and true negatives (TN), minimizing at the same time the number of false negatives (FN). Additionally, the proposed MBGAB procedure has been automated and can be easily reproducible in the same and other regions of the Earth for improving the detection of burned areas.

Declarations

- Funding
  This research was supported by the Spanish Research Agency (PID 2020-113125RB-I00/ MCIN/ AEI/ 10.13039/501100011033 project).
- Conflict of interest
  The authors declare no conflict of interest.
- Ethics approval
  Not applicable
- Consent to participate
  Not applicable
- Consent for publication
  Not applicable
- Availability of Data and Materials
  Data are of free access
- Code Availability
  R code for running MBAGB is accessible from https://github.com/spatialstatisticsupna/MBAGB
- Authors contribution
  All the authors have contributed equally to this work

References

[1] Valente, F., Laurini, M.: Spatio-temporal analysis of fire occurrence in australia. Stochastic Environmental Research and Risk Assessment **35**(9), 1759–1770 (2021)

[2] Paci, L., Gelfand, A.E., Beamonte, M.A., Rodrigues, M., Pérez-Cabello, F.: Space-time modeling for post-fire vegetation recovery. Stochastic Environmental Research and Risk Assessment **31**(1), 171–183 (2017)

[3] Giglio, L., Boschetti, L., Roy, D.P., Humber, M.L., Justice, C.O.: The collection 6 modis burned area mapping algorithm and product. Remote sensing of environment **217**, 72–85 (2018)

[4] EEDC: Earth Engine Data Catalog. [Online; accessed 19-January-2022]. https://modis.gsfc.nasa.gov/about/

[5] Landsat: Landsat Burned Area Essential Climate Variable. [Online; accessed 19-January-2022] (2021). http://dx.doi.org/10.5066/F73B5X76

[6] Landsat: Landsat Burned Area Science Products. [Online; accessed 19-January-2022] (2021). https://www.usgs.gov/core-science-systems/nli/landsat/landsat-burned-area

[7] Roteta, E., Bastarrika, A., Padilla, M., Storm, T., Chuvieco, E.: Development of a sentinel-2 burned area algorithm: Generation of a small fire database for sub-saharan africa. Remote sensing of environment **222**, 1–17 (2019)

[8] Zhang, Q., Ge, L., Zhang, R., Metternicht, G.I., Du, Z., Kuang, J., Xu, M.: Deep-learning-based burned area mapping using the synergy of sentinel-1&2 data. Remote Sensing of Environment **264**, 112575 (2021)

[9] Tanase, M.A., Belenguer-Plomer, M.A., Roteta, E., Bastarrika, A., Wheeler, J., Fernández-Carrillo, Á., Tansey, K., Wiedemann, W., Navratil, P., Lohberger, S., *et al.*: Burned area detection and mapping: Intercomparison of sentinel-1 and sentinel-2 based algorithms over tropical africa. Remote Sensing **12**(2), 334 (2020)

[10] Copernicus: Sentinel-3 BA products. [Online; accessed 18-January-2022] (2021). https://land.copernicus.eu/global/products/ba

[11] Jain, P., Coogan, S.C., Subramanian, S.G., Crowley, M., Taylor, S., Flannigan, M.D.: A review of machine learning applications in wildfire science and management. Environmental Reviews **28**(4), 478–505 (2020)

[12] Masoudvaziri, N., Ganguly, P., Mukherjee, S., Sun, K.: Impact of geophysical and anthropogenic factors on wildfire size: A spatiotemporal data-driven risk assessment approach using statistical learning. Stochastic Environmental Research and Risk Assessment, 1–27 (2021)

[13] Hu, X., Ban, Y., Nascetti, A.: Uni-temporal multispectral imagery for burned area mapping with deep learning. Remote Sensing **13**(8), 1509 (2021)

[14] Ramo, R., Chuvieco, E.: Developing a random forest algorithm for modis global burned area classification. Remote Sensing **9**(11), 1193 (2017). https://doi.org/10.3390/rs9111193

[15] Belgiu, M., Drăguţ, L.: Random forest in remote sensing: A review of applications and future directions. ISPRS journal of photogrammetry and remote sensing **114**, 24–31 (2016)

[16] Zhang, R., Qu, J.J., Liu, Y., Hao, X., Huang, C., Zhan, X.: Detection of burned areas from mega-fires using daily and historical modis surface reflectance. International Journal of Remote Sensing **36**(4), 1167–1187 (2015)

[17] Petropoulos, G.P., Kontoes, C., Keramitsoglou, I.: Burnt area delineation from a uni-temporal perspective based on landsat tm imagery classification using support vector machines. International Journal of Applied Earth Observation and Geoinformation **13**(1), 70–80 (2011)

[18] Mas JF, F.J.: The application of artificial neural networks to the analysis of remotely sensed data. Remote sensing of Environment **29**(3), 617–663 (2008)

[19] Pinto, M.M., Libonati, R., Trigo, R.M., Trigo, I.F., DaCamara, C.C.: A deep learning approach for mapping and dating burned areas using temporal sequences of satellite images. ISPRS Journal of Photogrammetry and Remote Sensing **160**, 260–274 (2020)

[20] Pinto, M.M., Trigo, R.M., Trigo, I.F., DaCamara, C.C.: A practical method for high-resolution burned area monitoring using sentinel-2 and viirs. Remote Sensing **13**(9), 1608 (2021)

[21] Knopp, L., Wieland, M., Rättich, M., Martinis, S.: A deep learning approach for burned area segmentation with sentinel-2 data. Remote Sensing **12**(15), 2422 (2020)

[22] Castelli, M., Vanneschi, L., Popovič, A.: Predicting burned areas of forest fires: an artificial intelligence approach. Fire ecology **11**(1), 106–118 (2015)

[23] Georganos, S., Grippa, T., Vanhuysse, S., Lennert, M., Shimoni, M., Wolff, E.: Very high resolution object-based land use–land cover urban classification using extreme gradient boosting. IEEE Geoscience and Remote Sensing Letters **15**(4), 607–611 (2018). https://doi.org/10.1109/LGRS.2018.2803259

[24] Hawbaker, T.J., Vanderhoof, M.K., Schmidt, G.L., Beal, Y., Picotte, J.J., Takacs, J.D., Falgout, J.T., Dwyer, J.L.: The Landsat Burned Area products for the conterminous United States: U.S. Geological Survey data release. (accesed on 25 August 2021) (2020). https://doi.org/10.5066/P9QKHKTQ

[25] Chen, T., Guestrin, C.: Xgboost. Proceedings of the 22nd ACM SIGKDD International Conference on Knowledge Discovery and Data Mining (2016). https://doi.org/10.1145/2939672.2939785

[26] Vhengani, L., Frost, P., Lai, C., Booi, N., van den Dool, R., Raath, W.: Multitemporal burnt area mapping using landsat 8: merging multiple burnt area indices to highlight burnt areas. In: 2015 IEEE International Geoscience and Remote Sensing Symposium (IGARSS), pp. 4153–4156 (2015). IEEE

[27] Reboredo, F., Challenges, F.: Forest context and policies in portugal **19**, 1–239 (2014)

[28] Giglio, L., Descloitres, J., Justice, C.O., Kaufman, Y.J.: An enhanced contextual fire detection algorithm for modis. Remote sensing of environment **87**(2-3), 273–282 (2003)

[29] VIIRS: Visible infrared imaging radiometer suite. [Online; accessed 09-January-2022] (2021). https://www.star.nesdis.noaa.gov/jpss/VIIRS.php

[30] Loboda, T., O'neal, K., Csiszar, I.: Regionally adaptable dnbr-based algorithm for burned area mapping from modis data. Remote sensing of environment **109**(4), 429–442 (2007)

[31] NASA: Fire information for resource managment system. (accesed on 25 August 2021) (2020). https://firms.modaps.eosdis.nasa.gov/map/

[32] EFFIS: European Forest Fire Information System (EFFIS). [Online; accessed 17-January-2022] (2021). https://effis.jrc.ec.europa.eu/

[33] Vermote, E.F., El Saleous, N.Z., Justice, C.O.: Atmospheric correction of modis data in the visible to middle infrared: first results. Remote Sensing of Environment **83**(1-2), 97–111 (2002)

[34] Harris, S., Veraverbeke, S., Hook, S.: Evaluating spectral indices for assessing fire severity in chaparral ecosystems (southern california) using modis/aster (master) airborne simulator data. Remote sensing **3**(11), 2403–2419 (2011)

[35] García, M.L., Caselles, V.: Mapping burns and natural reforestation using thematic mapper data. Geocarto International **6**(1), 31–37 (1991)

[36] Lutes, D.C., Keane, R.E., Caratti, J.F., Key, C.H., Benson, S. N.C. and-Sutherland, Gangi, L.J.: Landscape assessment:ground measure of severity, the composite burn index; and remote sensing of severity, the normalized burn ratio. FIREMON: Fire Effects Monitoring and Inventory System, USDA Forest Service, Rocky Mountain Research Station, Ogden, UT **1**, 1–51 (2006)

[37] Santana, N.C., de Carvalho Júnior, O.A., Gomes, R.A.T., Guimarães, R.F.: Burned-area detection in amazonian environments using standardized time series per pixel in modis data. Remote Sensing **10**(12), 1904 (2018)

[38] Hislop, S., Jones, S., Soto-Berelov, M., Skidmore, A., Haywood, A., Nguyen, T.H.: Using landsat spectral indices in time-series to assess

wildfire disturbance and recovery. Remote Sensing **10**(3) (2018)

[39] Giglio, L., Loboda, T., Roy, D.P., Quayle, B., Justice, C.O.: An active-fire based burned area mapping algorithm for the modis sensor. Remote sensing of environment **113**(2), 408–420 (2009)

[40] Trigg, S., Flasse, S.: An evaluation of different bi-spectral spaces for discriminating burned shrub-savannah. International Journal of Remote Sensing **22**(13), 2641–2647 (2001)

[41] McCarley, T.R., Smith, A.M., Kolden, C.A., Kreitler, J.: Evaluating the mid-infrared bi-spectral index for improved assessment of low-severity fire effects in a conifer forest. International Journal of Wildland Fire **27**(6), 407–412 (2018)

[42] Tucker, C.J.: Red and photographic infrared linear combinations for monitoring vegetation. Remote sensing of Environment **8**(2), 127–150 (1979)

[43] Mohler, R.L., Goodin, D.G.: A comparison of red, nir, and ndvi for monitoring temporal burn signature change in tallgrass prairie. Remote Sensing Letters **1**(1), 3–9 (2010)

[44] Chen, X., Vogelmann, J.E., Rollins, M., Ohlen, D., Key, C.H., Yang, L., Huang, C., Shi, H.: Detecting post-fire burn severity and vegetation recovery using multitemporal remote sensing spectral indices and field-collected composite burn index data in a ponderosa pine forest. International Journal of Remote Sensing **32**(23), 7905–7927 (2011)

[45] Van Wagtendonk, J.W., Root, R.R., Key, C.H.: Comparison of aviris and landsat etm+ detection capabilities for burn severity. Remote sensing of environment **92**(3), 397–408 (2004)

[46] Miller, J.D., Knapp, E.E., Key, C.H., Skinner, C.N., Isbell, C.J., Creasy, R.M., Sherlock, J.W.: Calibration and validation of the relative differenced normalized burn ratio (rdnbr) to three measures of fire severity in the sierra nevada and klamath mountains, california, usa. Remote Sensing of Environment **113**(3), 645–656 (2009)

[47] Eidenshink, J., Schwind, B., Brewer, K., Zhu, Z.-L., Quayle, B., Howard, S.: A project for monitoring trends in burn severity. Fire ecology **3**(1), 3–21 (2007)

[48] Friedman, J., Hastie, T., Tibshirani, R.: Additive logistic regression: a statistical view of boosting (with discussion and a rejoinder by the authors). The annals of statistics **28**(2), 337–407 (2000)

[49] Friedman, J.H.: Greedy function approximation: a gradient boosting machine. Annals of statistics, 1189–1232 (2001)

[50] Alnahit, A.O., Mishra, A.K., Khan, A.A.: Stream water quality prediction using boosted regression tree and random forest models. Stochastic Environmental Research and Risk Assessment, 1–20 (2022)

[51] R Core Team: R: A Language and Environment for Statistical Computing, Vienna, Austria (2021). https://github.com/spatialstatisticsupna/rsat/

[52] Pérez-Goya, U., Montesino-SanMartin, M., Militino, A.F., Ugarte, M.D.: rsat: Dealing with Multiplatform Satellite Images. R package version 0.1.14. (2020). https://github.com/spatialstatisticsupna/rsat

[53] Yao, R., Wang, L., Huang, X., Sun, L., Chen, R., Wu, X., Zhang, W., Niu, Z.: A robust method for filling the gaps in modis and viirs land surface temperature data. IEEE Transactions on Geoscience and Remote Sensing **59**(12), 10738–10752 (2021). https://doi.org/10.1109/TGRS.2021.3053284

[54] Militino, A.F., Ugarte, M.D., Pérez-Goya, U., Genton, M.G.: Interpolation of the mean anomalies for cloud filling in land surface temperature and normalized difference vegetation index. IEEE Transactions on Geoscience and Remote Sensing **57**(8), 6068–6078 (2019). https://doi.org/10.1109/TGRS.2019.2904193

[55] Militino, A.F., Ugarte, M., Montesino, M.: Filling missing data and smoothing altered data in satellite imagery with a spatial functional procedure. Stochastic Environmental Research and Risk Assessment **33**(10), 1737–1750 (2019)

[56] Guindon, B., Zhang, Y.: Application of the Dice Coefficient to Accuracy Assessment of Object-Based Image Classification. Canadian Journal of Remote Sensing **43**(1), 48–61 (2017). https://doi.org/10.1080/07038992.2017.1259557. Publisher: Taylor & Francis

[57] Phelps, N., Woolford, D.G.: Guidelines for effective evaluation and comparison of wildland fire occurrence prediction models. International journal of wildland fire **30**(4), 225–240 (2021)

[58] Hawbaker, T.J., Vanderhoof, M.K., Schmidt, G.L., Beal, Y.-J., Picotte, J.J., Takacs, J.D., Falgout, J.T., Dwyer, J.L.: The landsat burned area algorithm and products for the conterminous united states. Remote Sensing of Environment **244**, 111801 (2020)